Nuclear Materials and Energy 9 (2016) 422–429

Contents lists available at ScienceDirect

Nuclear Materials and Energy

journal homepage: www.elsevier.com/locate/nme

Manufacturing and testing of self-passivating tungsten alloys of different composition

A. Calvo[a], C. García-Rosales[a,*], F. Koch[b], N. Ordás[a], I. Iturriza[a], H. Greuner[b], G. Pintsuk[c], C. Sarbu[d]

[a] Ceit-IK4 Technology Center and Tecnun (University of Navarra), E-20018 San Sebastián, Spain
[b] Max-Planck-Institut für Plasmaphysik, D-85748 Garching, Germany
[c] Forschungszentrum Jülich GmbH, D-52425 Jülich, Germany
[d] National Institute of Materials Physics, R-077125 Magurele-Bucharest, Romania

ARTICLE INFO

Article history:
Available online 22 June 2016

Keywords:
Tungsten alloys
Oxidation resistance
Armour material
Mechanical alloying
HIP

ABSTRACT

Self-passivating tungsten based alloys for the first wall armour of future fusion reactors are expected to provide a major safety advantage compared to pure tungsten in case of a loss of coolant accident with simultaneous air ingress, due to the formation of a stable protective scale at high temperatures in presence of oxygen which prevents the formation of volatile and radioactive WO_3.

Bulk W-15Cr, W-10Cr-2Ti and W-12Cr-0.5Y alloys were manufactured by mechanical alloying followed by can encapsulation and HIP. This route resulted in fully dense materials with nano-structured grains. The ability of Ti and especially of Y to inhibit grain growth was observed in the W-10Cr-2Ti and W-12Cr-0.5Y alloys. Besides, Y formed Y-rich oxide nano-precipitates at the grain boundaries, and is thus expected to improve the mechanical behaviour of the Y-containing alloy. Isothermal oxidation tests at 800 °C (1073 K) and oxidation tests under accident-like conditions revealed that the W-12Cr-0.5Y alloy exhibits the best oxidation behaviour of all alloys, especially in the accident-like scenario. Preliminary HHF tests performed at GLADIS indicated that the W-10Cr-2Ti alloy is able to withstand power densities of 2 MW/m^2 without significant damage of the bulk structure. Thermo-shock tests at JUDITH-1 to simulate mitigated disruptions resulted in chipping of part of the surface of the as-HIPed W-10Cr-2Ti alloy. An additional thermal treatment at 1600 °C (1873 K) improves the thermo-shock resistance of the W-10Cr-2Ti alloy since only crack formation is observed.

© 2016 The Authors. Published by Elsevier Ltd.
This is an open access article under the CC BY-NC-ND license (http://creativecommons.org/licenses/by-nc-nd/4.0/).

1. Introduction

In future fusion reactors such as DEMO, a potential loss-of-coolant accident with simultaneous air ingress into the vacuum vessel would involve temperatures of the in-vessel components above 1000°C (1273 K) because of the decay heat [1]. Under this situation, the use of pure tungsten, presently planned for the blanket protecting first wall armour [2], represents an important safety issue due to its high oxidation rate at high temperatures, which would lead to full oxidation of the armour layer. Since tungsten oxide is rather volatile at the involved temperatures, part of the tungsten would be mobilized with the consequent release of highly activated species [3]. A possible way to avoid the risk of radioactive release during such a scenario would be the addition of oxide forming alloying elements to tungsten, resulting in the formation of a stable protective oxide scale at high temperatures in presence of oxygen. During normal operation, the surface of this self-passivating alloy will consist of pure tungsten, owing to preferential sputtering of the alloying elements.

In previous works [4-6], different bulk tungsten alloys of the systems W-Cr-Si and W-Cr-Ti were manufactured by mechanical alloying (MA) and densification by Hot Isostatic Pressing (HIP). The addition of Cr and Si or Ti as alloying elements resulted in a reduction of the oxidation rate by several orders of magnitude at temperatures up to 1000°C (1273 K) compared to pure tungsten, due to the growth of a protective oxide layer [4,7-9]. Nevertheless, Si tends to form brittle intermetallics with detrimental effect on the workability of the alloys and Ti contributes to enhance tritium retention [10]. Both reasons have motivated the search for alternative systems avoiding Si [6,8] and Ti as alloying elements. Binary W-Cr alloys represent a feasible alternative; such alloys have

* Corresponding autor.
E-mail address: cgrosales@ceit.es (C. García-Rosales).

http://dx.doi.org/10.1016/j.nme.2016.06.002
2352-1791/© 2016 The Authors. Published by Elsevier Ltd. This is an open access article under the CC BY-NC-ND license (http://creativecommons.org/licenses/by-nc-nd/4.0/).

been subject to several investigations aiming at improving the oxidation behaviour of tungsten [11] and at enhancing its irradiation resistance by nano-structuring [12]. A recent study [13] has been focused on the determination of the optimum Cr concentration range in W-Cr binary thin film alloys for achieving lower oxidation rates though the development of an effective protective layer, leading to values between 10 and 16 wt.%. In addition, thin films of the system W-Cr-Y recently produced by magnetron sputtering were shown to exhibit lower oxidation rate by isothermal oxidation than similar alloys of the W-Cr-Ti system [14]. The high affinity of Y to oxygen can contribute to reduce the oxygen impurity content from the grain boundaries (GB) due to its oxygen getter effect, thus contributing to reduce the ductile-to-brittle transition temperature (DBTT) of tungsten [15]. Furthermore, the addition of up to 1.5 wt.% Y to tungsten inhibits grain growth resulting in grain size refinement [15-17] due to the pinning effect of finely dispersed Y_2O_3 nanoparticles in the W matrix. From all previously mentioned, alloys of the W-Cr-Y system appear to be especially attractive for first wall armour application.

In this work, alloys with different compositions of the system W-Cr-Ti as well as new binary and ternary systems, W-Cr and W-Cr-Y respectively, are studied. The alloys are manufactured by MA followed by can encapsulation and HIP. The W–Cr phase diagram is characterized by a miscibility gap below 1677°C (1950 K), leading to decomposition of the high-temperature bcc solid solution into a Cr-rich and a W-rich solid solution phases, known as spinodal decomposition [18]. In the case of the W-Cr-Ti samples, a subsequent thermal treatment at a temperature above the corresponding decomposition temperature is performed after HIP to achieve a single bcc phase microstructure. In this way the presence of the Cr-rich phase, more prone to oxidation than the W-rich phase [4,9], is avoided, and the oxidation resistance of the alloy is expected to be improved; the presence of a single W-rich bcc phase is also preferred in view of an improved mechanical behaviour, since misfit strains and thermal stresses induced by the second phase are avoided. Microstructural investigations, thermal conductivity and microhardness of the alloys after HIP and after the subsequent thermal treatment (only for the W-Cr-Ti system) are presented. A summary of the results of different tests is shown: oxidation tests at various conditions, high heat flux (HHF) tests at GLADIS (Garching Large Divertor Sample Test Facility) [19] as a first "proof of principle" test according to the expected load at the blanket first wall, and thermo-shock tests at JUDITH-1 (Juelich Divertor Test Facility Hot Cells) [20] to simulate conditions under mitigated disruptions in a DEMO-like device.

2. Experimental details

Elemental powders of pure W (99.95%, 15-30 µm), Cr (99.95%, 74 µm), Ti (99.5%, 40 µm) and Y (99.9%, 20-30 µm) were used to produce samples of composition W-10Cr-2Ti, W-15Cr and W-12Cr-0.5Y in wt.% (corresponding to W-27Cr-6Ti, W-38Cr and W-32Cr-0.8Y in at.%). The starting powders were mechanically alloyed under Ar in a planetary ball mill Retsch PM400 using WC grinding jars and balls. The MA parameters were those found as optimum for W-Cr-Ti systems in previous works [4-5]. Metallic capsules of Ø 15 mm and 40 mm height filled with the alloyed powder were evacuated, degassed at high vacuum, sealed and HIPed at 1220 °C (1493 K) for 2 h at 150 MPa. The oxygen and nitrogen contents after MA and HIPing were determined using the inert gas fusion method (ASTM E1569, measured with a LECO TC-400), and the carbon content by the combustion method (ASTM E1019, measured with a LECO CS-200). Powders and bulk samples were characterized by field emission gun SEM (FEG-SEM), energy dispersive X-ray spectroscopy (EDS) and X-ray diffraction (XRD). The relative density of the samples was determined from the geometrical and theoretical densities. The average grain size of the dense materials was determined by quantitative metallography. Vickers microhardness of the HIPed materials was measured applying a load of 0.5 kg for 5 seconds. The thermal conductivity up to 900 °C (1173 K) was obtained by the laser flash method. A thermal treatment (TT) on W-10Cr-2Ti HIPed samples was performed at 1600 °C (1873 K) in H_2.

Isothermal oxidation tests at 800°C (1073 K) for up to 60 h were performed by thermogravimetric analysis (TGA). Besides, tests under accident-like conditions were also performed. These tests consist of a preheating in Ar up to 600°C (873 K) followed by oxidation in a mixture of 80 vol.% argon and 20 vol.% oxygen (H_2O content $\leq$ 3 ppm) at linear increasing temperature from 600 to 1000°C (873 to 1273 K) during about 17 h, two isothermal oxidation steps in air at 1000°C (1273 K) for 1 h, each of them followed by isothermal steps in Ar at 1000°C (1273 K) for 1 h, and cooling down in Ar. Preliminary HHF tests at GLADIS were performed on an as-HIPed W-10Cr-2Ti sample of dimensions $10 \times 5 \times 6$ mm^3 by applying 30 pulses of 2 MW/m² for 2 s with a neutral hydrogen beam, according to the power load expected at the first wall [2]. The 2 s pulse duration was chosen to achieve 1000°C (1273 K) surface temperature at the end of the pulse. The samples were not actively cooled and thus, a cooling time of 7 minutes after each pulse was required to prevent overheating. The adiabatic loading generates high temperature gradients, which allow a preliminary assessment of the thermo-mechanical behaviour of the material. Besides, the relatively long cooling time permits to evaluate the thermal stability of the bulk structure and possible grain growth.

Thermo-shock tests were performed at the electron beam facility JUDITH-1 [20] on an as-HIPed W-10Cr-2Ti sample and on a W-10Cr-2Ti sample after HIP and TT at 1600°C (1873 K). The samples, of dimensions $10 \times 10 \times 4$ mm^3, were exposed to 100 pulses of a power density of 0.38 GW/m^2 for 1 ms at a base temperature of 400°C (673 K). These conditions correspond to a heat flux factor (HF) of 12 MW/m^2 · s$^{1/2}$ (heat flux factor $= P_{ab}\sqrt{t}\cdot$) which is a measure of the temperature increase:

$$\Delta T = 2 \cdot P_{ab} \sqrt{\frac{t}{\pi \cdot \lambda \cdot c_p \cdot \rho}}$$

Therein, P_{ab} is the absorbed power density, t the pulse duration and λ, ρ and c are thermal conductivity, density and specific heat, respectively. The base temperature is achieved by means of a heated graphite holder, which is electronically controlled via a thermocouple. To ensure an almost homogeneous loading, a small area (4×4 mm^2) was scanned with a focused electron beam (beam diameter ~1 mm) at very high scanning frequencies ($f_x = 40$ kHz, $f_y = 31$ kHz). After exposure, the samples were investigated by optical microscopy and SEM. Additionally, the cross section of the samples was analyzed by metallography to study the crack propagation into the bulk material.

3. Results and discussion

Mechanically alloyed powders of composition W-15Cr, W-10Cr-2Ti and W-12Cr-0.5Y in wt.% were can encapsulated and HIPed at 1220 °C (1493 K) for 2 h achieving relative densities above 99%, i.e. the material obtained can be considered fully dense within the experimental error. In Table 1 the relative density as well as the O, C and N contents of the as-HIPped materials are shown, which are comparable to those reported in previous works [5,6].

3.1. Microstructure

The microstructure of the three alloys is compared in Fig. 1. A very fine and homogeneous microstructure can be appreciated in all systems, with two main phases identified by EDS as a W-rich phase with Cr in solution (bright grey majority phase) and a

Table 1
Relative density, impurities content, average grain size and microhardness of the materials produced by MA+HIP. For comparison, the microhardness of pure polycrystalline tungsten at the same average grain size is included.

	Relative density (%)	Impurities (ppm)			Average grain size (nm)	Microhardness (HV 0.5)	Microhardness of pure W [25] (HV)
		O	N	C			
W-15Cr	99.5	1000 ± 100	70 ± 20	380 ± 10	190 ± 2	997 ± 2	1076
W-10Cr-2Ti	100	1100 ± 100	110 ± 10	140 ± 20	110 ± 6	1206 ± 10	1304
W-12Cr-0.5Y	99	1300 ± 200	90 ± 10	170 ± 10	87 ± 2	1228 ± 5	1422

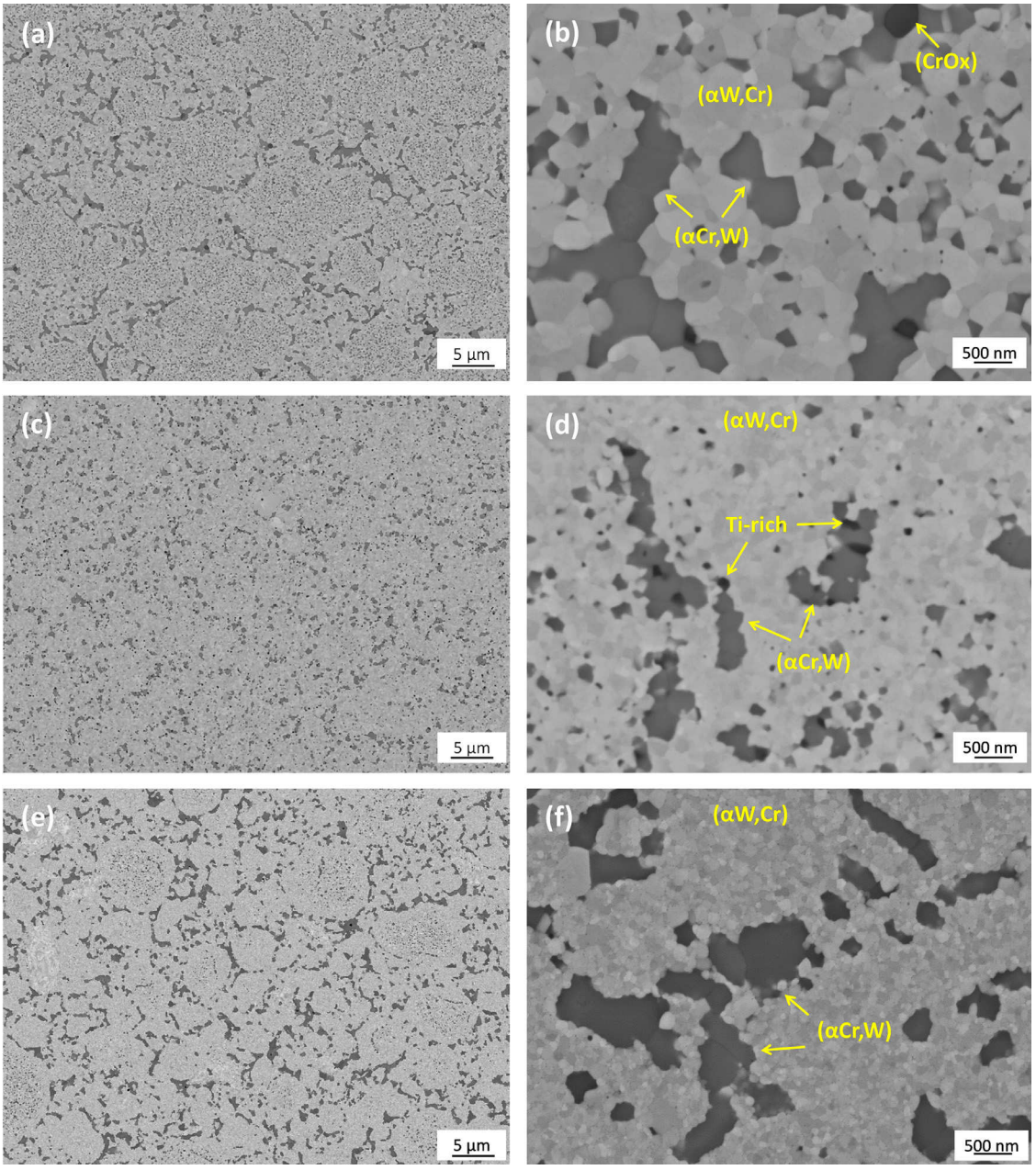

Fig. 1. FEG-SEM images of W-15Cr (a-b), W-10Cr-2Ti (c-d) and W-12Cr-0.5Y (e-f) alloys after HIP at 1220 °C (1473 K).

Cr-rich phase with W in solution (dark grey discontinuous phase). The compositions of these bcc phases (αW, Cr) and (αCr, W) after HIP were estimated from the shift of the XRD peaks (Fig. 2) using the Vegard's law [21]. The amount of Cr dissolved in W is about 5 wt.% (16 at.%) whereas the amount of W in solid solution in Cr is about 41 wt.% (17 at.%), which is consistent with the compositions predicted by the W-Cr phase diagram [18] at 1220 °C (1493 K) (Fig. 3). The prior particle boundaries (PPBs) of the powders after MA can be distinguished (Fig. 1(a), (c) and (e)) due to the preferential presence in these areas of the largest grains of the Cr-rich phase. This Cr preferential enrichment of PPBs is more pronounced in the alloys with the highest Cr content (W-15Cr and W-12Cr-0.5Y). Cr exhibits a higher affinity to oxygen than W in the temperature range RT-1600 °C. The Ti-rich phase in

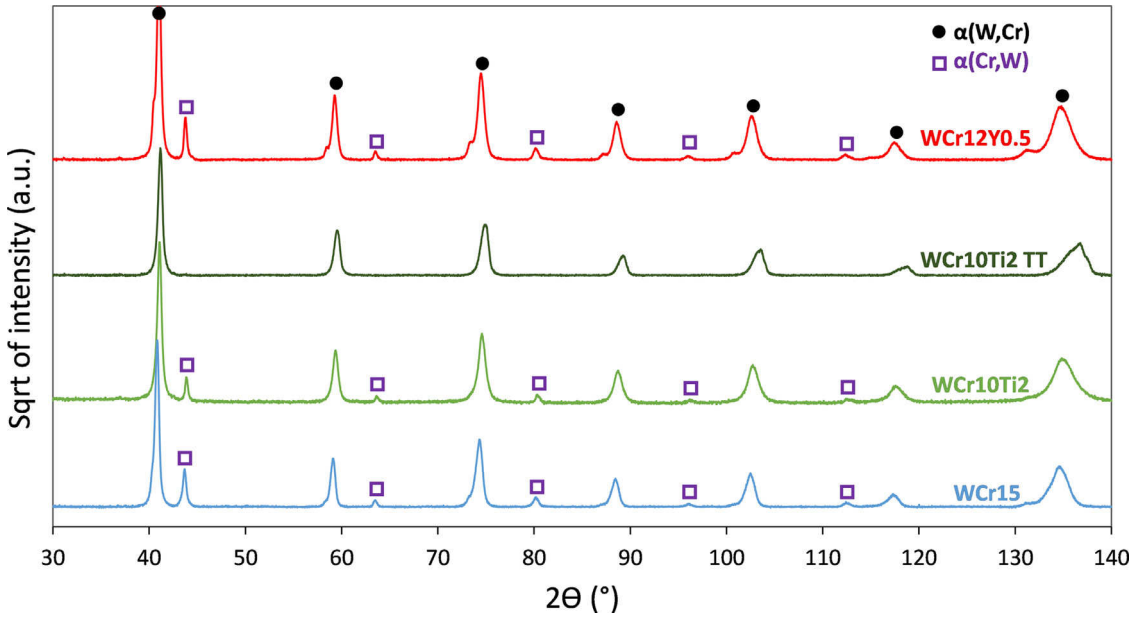

Fig. 2. XRD spectra of W-15Cr, W-10Cr-2Ti and W-12Cr-0.5Y alloys after HIP at 1220 °C (1473 K) and W-10Cr-2Ti alloy after HIP at 1220 °C + TT at 1600 °C (1873 K).

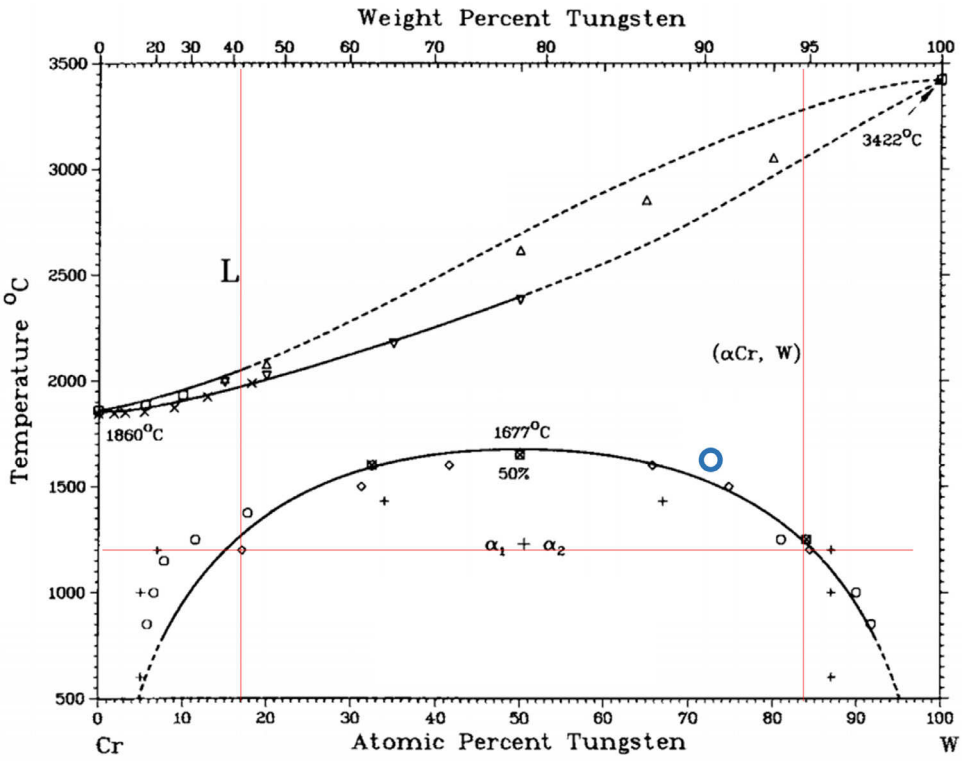

Fig. 3. W-Cr phase diagram [18] indicating the composition of the bcc (αW,Cr) and (αCr,W) phases after HIP deduced from the peak positions of the corresponding XRD peaks (red lines). The composition of the single bcc phase expected after TT at 1600°C (1874 K) is also indicated (blue dot). (For interpretation of the references to colour in this figure legend, the reader is referred to the web version of this article).

W-10Cr-2Ti is also preferentially located close to the PPBs and adjacent to largest grains of the Cr-rich phase, which is also consistent with the highest thermal stability of its oxides, compared to those of Cr and W. It is likely that the PPBs, which exhibit higher oxygen content (probably in form of Cr_2O_3 after MA) than the interior of the particles, act as nucleation points for the (αCr, W) phase. The W-15Cr and W-10Cr-2Ti alloys show ultra-fine grained structures with average grain size below 200 nm and 120 nm respectively, whereas the W-12Cr-0.5Y alloy exhibits a nanocrystalline microstructure with average grain size below 100 nm. This difference in the grain size between the binary and ternary systems is a clear indication of the ability of Ti and especially of Y to inhibit grain growth, which is well known to be beneficial for increasing the strength and reducing the DBTT [22,23], since grain refinement raises the GB area, thus reducing the concentration of GB impurities and strengthening the GB. In addition to the main phases, the darkest phase was identified by EDS in the W-15Cr alloy as Cr-oxide, and in the W-10Cr-2Ti

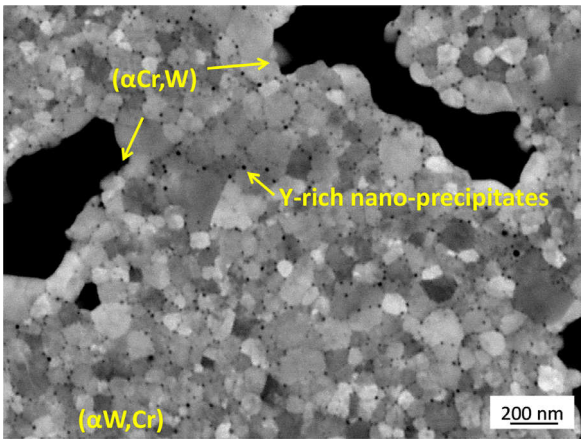

Fig. 4. Microstructure of W-12Cr-0.5Y after HIP at 1220 °C (1493 K) at high magnification.

alloy as a Ti-rich phase containing oxygen, as mentioned above (Fig. 1(b) and (d), respectively). In the same way, Y-rich oxide nano-particles of about 15 nm size can be observed in the W-12Cr-0.5Y alloy at highest magnification (Fig. 4). Considering the highest oxygen affinity of Y, compared to the other alloying elements, and the oxygen present in the alloy after HIP (0.13 wt.%, see Table 1), it can be easily derived that almost all the Y of this alloy is oxidized as Y_2O_3 nanoparticles. It becomes clear that Y has an oxygen getter effect, contributing to remove oxygen from the GBs during HIPing due to the decomposition of less stable oxides, which are responsible for the low temperature brittleness of W alloys [24]. The Y-rich ODS-like phase, which is stable up to very high temperatures, is expected to improve the hot strength and creep resistance of the alloy and to decrease the DBTT [15-17]. More work is required to identify by TEM the composition and crystalline structure of this ODS-like phase and of the other minority phases.

A TT at 1600 °C (1873 K) was performed on the W-10Cr-2Ti HIPed samples, i.e. above the spinodal decomposition (see Fig. 3), aiming at producing a single phase material without the presence of the Cr-rich phase, more prone to oxidation, at the risk of increasing the grain size. In Fig. 5 the microstructure of the W-10Cr-2Ti alloy after HIP and TT is shown at two different magnifications. It consists of a (αW,Cr) main phase with minor presence of (αCr,W) and Ti-rich phases with finer grain size. The observed microstructure is in line with the corresponding XRD spectrum shown in Fig. 2, where the (αCr,W) phase is no longer detected due to its limited presence. In this spectrum the peaks of the W-rich phase are shifted to higher 2θ values, as expected, due to the higher amount of Cr in solid solution, but their asymmetric shape including intensity of the peaks from the composition previous to the TT let assume that a homogeneous phase composition has not yet been achieved. The obtained microstructure is also consistent with the W-Cr phase diagram (Fig. 3), where a unique phase is present at 1600 °C (1873 K). Grain growth up to approximately 1 µm can be observed in the (αW,Cr) phase after TT and Ti-rich nano-precipitates of about 20 nm can be also distinguished at the GB. Again, further work is required to identify by TEM the composition of these nano-precipitates.

3.2. Microhardness and thermal conductivity

The Vickers microhardness values of the HIPed materials are reported in Table 1. As a reference, the microhardness of pure polycrystalline tungsten at the corresponding average grain size is included, taking into account its Hall-Petch relationship [25]. The hardness of the three alloys are slightly lower than that of pure tungsten at the same average grain size, as might be expected because of the presence of a Cr-rich phase with lower hardness than W. These values indicate a clear effect of grain size on hardening in the investigated alloys.

In the case of the W-10Cr-2Ti alloy after TT, a decrease in Vickers microhardness from 1206 to 970 $HV_{0.5}$ was observed, which can be also mainly explained by the grain size increase.

The thermal conductivity of the W-15Cr and W-10Cr-2Ti alloys from RT to 900 °C (1173 K) is shown in Fig. 6. The binary system exhibits higher values than the ternary one, probably due to the fact that in the W-10Cr-2Ti alloy part of the Ti is in solid solution in the (αW,Cr) and (αCr,W) phases, as confirmed by EDS analysis performed on a foil of this alloy by TEM. The thermal conductivity of the W-10Cr-2Ti alloy after HIP+TT is similar to, though slightly lower than, the one after HIP.

3.3. Oxidation tests

Isothermal oxidation tests at 800 °C (1073 K) for 60 hours and accident-like conditions oxidation tests up to 1000 °C (1273 K) were performed on the three systems including the heat treated samples of the W-10Cr-2Ti alloy. The mass increase during isothermal oxidation (Fig. 7(a)) appears to follow a linear rate law in all cases; the binary W-15Cr system starts with a higher linear rate and changes to a lower rate after about 10 h. The binary system exhibit a significantly higher oxidation rate under isothermal conditions that the ternary alloys. There is no significant difference between the isothermal behaviours of the two W-10Cr-2Ti alloys (as HIPed and HIP+TT), while the W-12Cr-0.5Y alloy shows the lowest oxidation rate. The results obtained for the W-10Cr-2Ti alloys are in agreement with those obtained in previous work for a similar composition [8].

In contrast to the isothermal oxidation at 800°C (1073 K), the mass increase at the isothermal segments during the accident-like tests (Fig. 7(b)) follows a parabolic rate law for all alloys. In this case the thermal treated W-10Cr-2Ti alloy exhibits a notably lower mass gain than the as-HIPed alloy due to the almost complete absence of the Cr-rich phase. Surprisingly, the binary W-15Cr alloy shows a significantly lower mass gain under accident-like conditions than the two W-10Cr-2Ti alloys. The excellent oxidation resistance of this binary alloy under accident-like conditions makes the W-15Cr alloy a promising first-wall armour material in view of keeping the hydrogen retention low. Even more promising is the W-12Cr-0.5Y alloy, which exhibits the lowest mass gain of all alloys during accident-like conditions. Another important observation is the fact that in the isothermal segments without oxygen there is no mass loss, indicating that there is no evaporation of tungsten oxides. The analysis of the oxide scales after the tests under isothermal and accident-like conditions and the elucidation of the underlying oxidation mechanisms will be addressed in a future work.

3.4. High heat flux and thermo-shock tests

Preliminary HHF tests consisting of 30 pulses of 2 MW/m^2 for 2 seconds were performed on as-HIPed W-10Cr-2Ti samples at GLADIS. The mean particle energy of the H beam was 9 keV and the total applied fluence 1×10^{23} m^{-2}. This corresponds to a calculated erosion in pure W of 3 nm due to physical sputtering, while the erosion in Cr is about two times the one of W. Fig. 8 shows the affected surface layer after the thermal load. The alloy withstood the load without significant damage of the bulk structure; only surface erosion of the Cr-rich phase can be observed, as indicated in the red circle of Fig. 8(a). This can be partly explained by the higher erosion rate of Cr compared to W. Other additional reasons for the higher erosion of Cr can be its high vapour pressure.

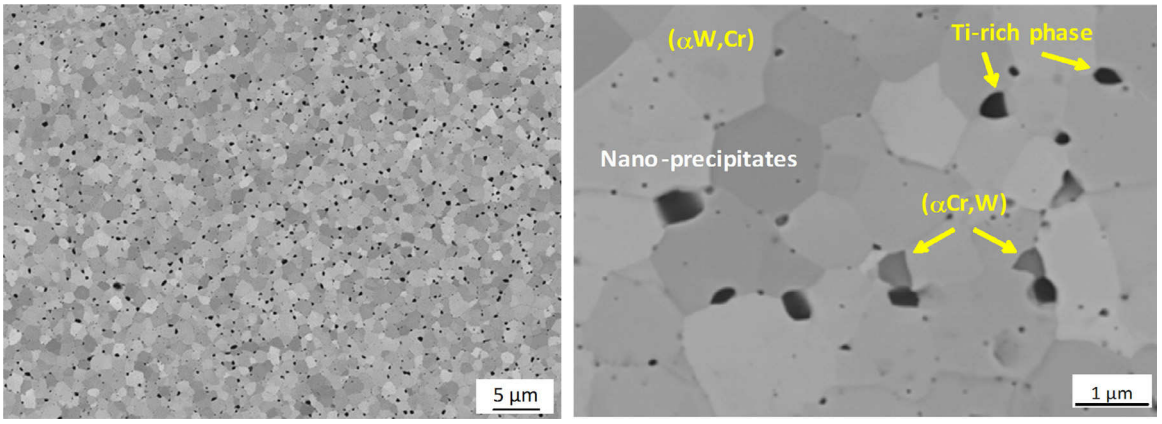

Fig. 5. FEG-SEM images of the W-10Cr-2Ti alloy after HIP at 1220 °C (1493 K) and subsequent TT at 1600 °C (1873 K).

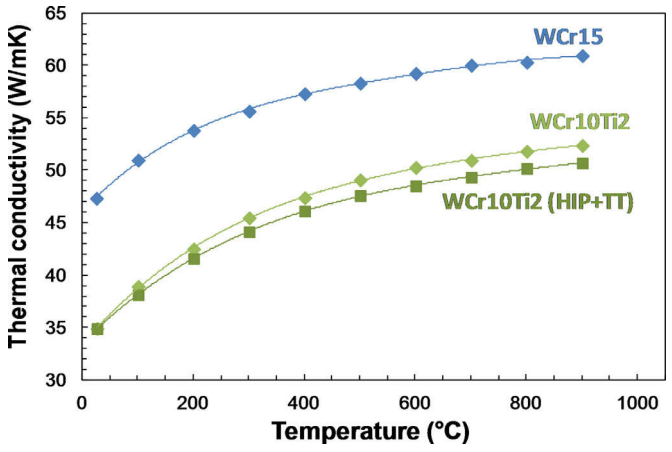

Fig. 6. Thermal conductivity of the as-HIPed W-15Cr and W-10Cr-2Ti alloys and of the W-10Cr-2Ti alloy after HIP + TT as a function of temperature.

Further investigation of the material behaviour under heat and H particle loading is required to assess these observations. Taking this result into account, one can assert that a thermal treatment at 1600°C (1873 K) may be beneficial as practically only a (αW, Cr) phase is present in the material. In any case, these preliminary results indicate that the W-10Cr-2Ti alloy has the potential to be used as self-passivating plasma-facing material for first-wall application.

An as-HIPed W-10Cr-2Ti sample and a W-10Cr-2Ti sample after HIP and TT at 1600°C (1873 K) were exposed to 100 heat pulses of 0.38 GW/m^2 for 1 ms at a base temperature of 400°C (673 K) at the electron beam facility JUDITH-1. These heat loads simulate the conditions expected during ELMs in the divertor, while the load at the blanket first wall during ELMs will be significantly lower. Nevertheless, in a DEMO-like device massive gas injection will be used to mitigate or avoid disruptions; this gas injection will produce photon flashes which result in very similar loads at the first wall to those applied here in a single pulse. Thus, this test simulates the load at the first wall after 100 mitigated disruptions.

Taking into account the heat flux factor of 12 MW/m^{2}s$^{1/2}$ and the thermo-physical properties of the materials at the base temperature of 400°C (673 K), a temperature increase of about 1150 K is expected. The fast increase in surface temperature during thermo-shock loading and the formation of a steep temperature gradient causes high compressive stresses in the small heat affected zone. At temperatures above the DBTT the ductility of the material should be able to compensate the plastic deformation and the induced stresses resulting in an increased surface roughness. In contrast, at temperatures below the DBTT the risk of brittle crack formation increases due to fast cooling across the DBTT. In the present case, part of the surface of the as-HIPed W-10Cr-2Ti chipped off after loading (Fig. 9(a)). On the contrary, there was

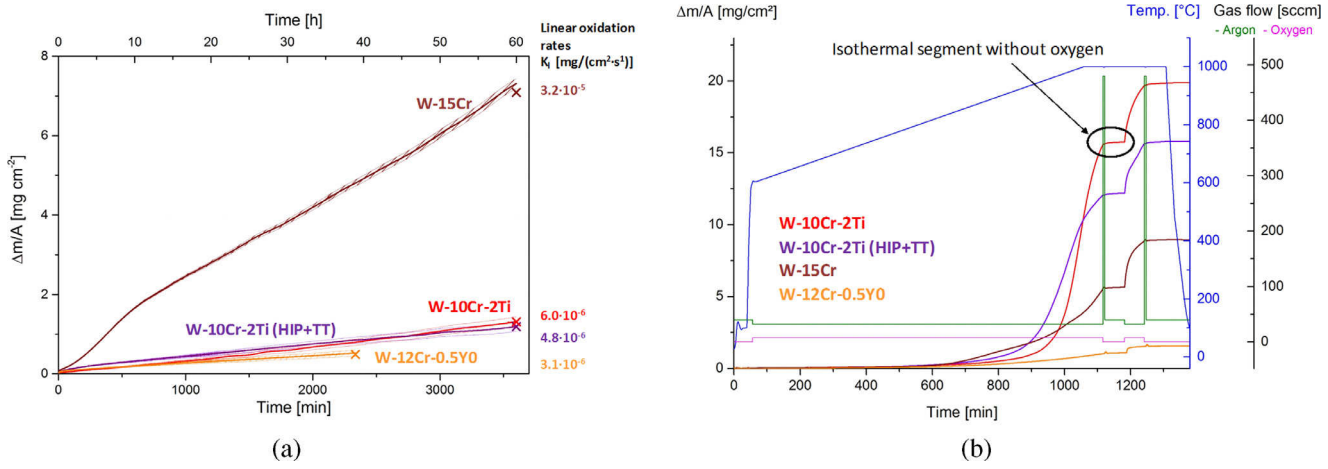

Fig. 7. Mass increase per unit area during isothermal oxidation test at 800 °C (1073 K) for up to 60 h (a) and during accident-like conditions test (b). The corresponding linear oxidation rates after the isothermal tests are indicated at the right hand side of (a). The "X" in (a) corresponds to the mass increase after the experiments as measured with a micro balance. The shaded areas are the possible drift of the thermo-balance according to the manufacturer.

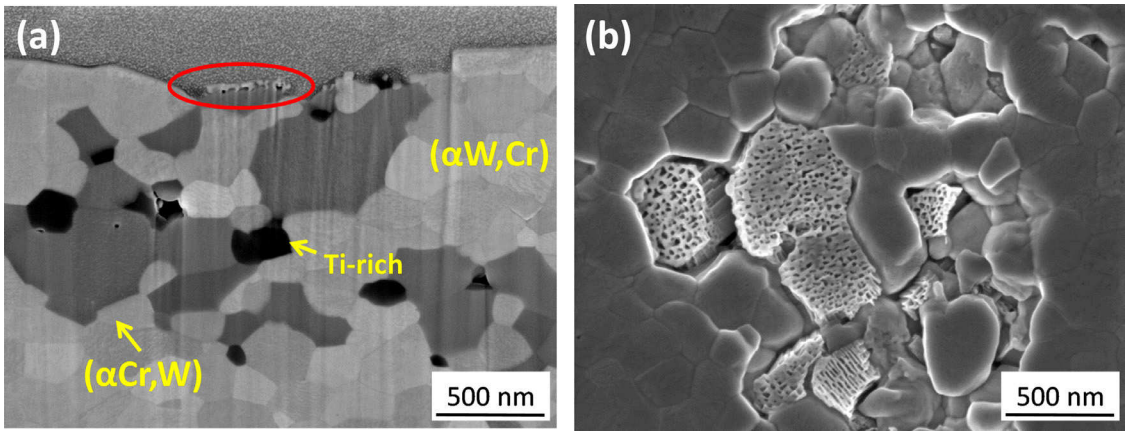

Fig. 8. FIB cross section (a) and surface view (b) after HHF tests on as-HIPed W-10Cr-2Ti at GLADIS.

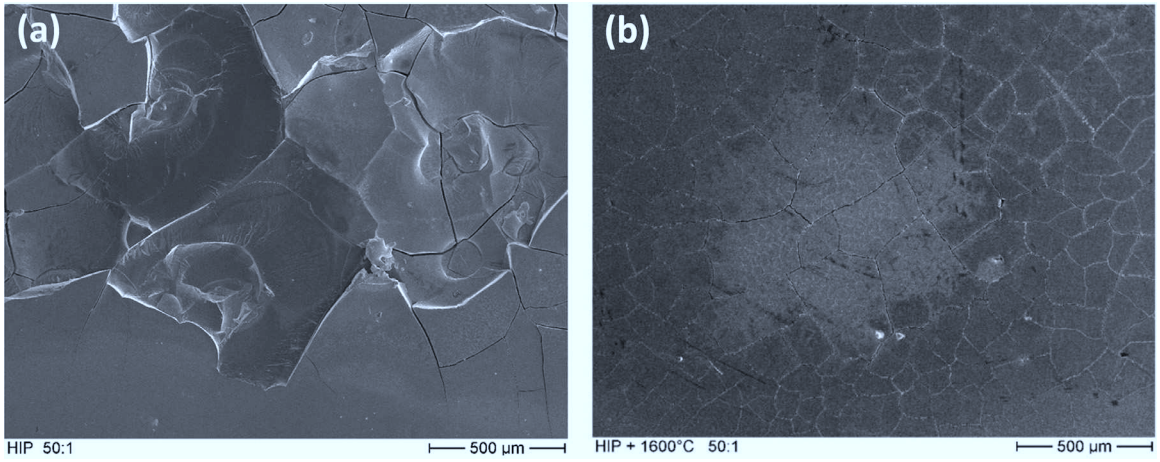

Fig. 9. SEM images of (a) as-HIPed W-10Cr-2Ti alloy and (b) HIPed+TTed W-10Cr-2Ti alloy after loading in JUDITH-1 with 100 ELM-like pulses.

no chipping after loading at the alloy after HIP and TT but only cracking (Fig. 9(b)) with crack depths varying from 100 to several 100 µm. The cracks were not only perpendicular but also parallel to the sample surface. In both cases brittle crack formation occurs.

Both alloys have practically the same thermal conductivity. Thus, the reason for a better behaviour of the alloy with additional TT has to lie in the different microstructure of both alloys and more precisely in the presence of practically one single bcc phase in the alloy after the TT, compared to the as-HIPed material exhibiting two bcc phases. Even though the smaller grain size of the as-HIPed material should result in a higher strength, it becomes clear that the second (αCr,W) bcc phase induces misfit strains and thermal stresses during repeated thermo-shock loading, resulting in a reduced thermo-shock resistance.

Nevertheless, the results confirm that the materials are brittle up to high temperatures, as already measured in previous works for the as-HIPed alloy [5,6] where the DBTT was found to be of the order of 900 °C (1173 K). The reasons for such a high DBTT are various: a high content of interstitials, especially oxygen (see Table 1), which segregate mainly at the GB and lead to a weakening of the GB strength. The extremely small grain size leading to a very high GB area of the as-HIPed alloy do not compensate for the high amount of oxygen. Besides, alloying with a relative large Cr amount results in embrittlement, if no cold working is performed to increase the amount of edge dislocations, which are known to reduce the DBTT [23].

Taking the previous results into consideration, the addition of small amounts of Y as alloying element is expected to be very beneficial in view of removing the oxygen from the GB by forming Y-rich oxide nanoparticles and hence contributing to reduce the DBTT. Y-rich oxide nanoprecipitates should also contribute to reinforce the material, increasing the high temperature strength and creep resistance.

The simulated heat loads corresponds to the values expected at the blanket first wall during 100 mitigated disruptions in a DEMO-like device. This means that a reduced DBTT or an increase in toughness may be necessary to allow the use of such an alloy at the first wall of DEMO. It needs to be assessed whether the expected beneficial effect of Y does provide the required improved mechanical properties to withstand the thermo-shock loading during mitigated disruptions. Furthermore, the impact of the observed crack network has still to be assessed in more detail taking into account that the armour material has no structural function for the blanket first wall.

4. Conclusions

Self-passivating bulk W-15Cr, W-10Cr-2Ti and W-12Cr-0.5Y alloys were manufactured by MA followed by can encapsulation and HIP. This powder metallurgical route resulted in fully dense materials with a very fine and homogeneous microstructure consisting of two main bcc phases, (αW,Cr) and (αCr, W). The ability of Ti and especially of Y to inhibit grain growth was observed in W-10Cr-2Ti and W-12Cr-0.5Y alloys. Furthermore, Y is effective in removing oxygen from the GB forming an ODS-like phase of Y-rich oxide nano-precipitates, and it is thus expected to contribute to a

reduction of the DBTT and to increased high temperature strength and creep resistance.

During isothermal oxidation at 800°C (1073 K) all alloys showed a linear rate law, while during accident-like conditions up to 1000°C (1273 K) they presented a parabolic rate law. The binary W-15Cr alloy exhibited significantly lower mass gain under accident-like conditions than the W-10Cr-2Ti alloy, making it a promising material in view of keeping the hydrogen retention low. Even more promising is the W-12Cr-0.5Y alloy, which exhibits the lowest mass gain of all alloys, especially under accident-like conditions.

Preliminary HHF tests performed at GLADIS indicated that the W-10Cr-2Ti alloy is able to withstand power densities of 2 MW/m^2 without significant damage of the bulk structure; however, surface erosion of the Cr-rich phase is observed. This result let assume that a thermal treatment at 1600°C (1873 K) may be beneficial in view of avoiding this second phase. The result confirms the potential of the W-10Cr-2Ti alloy as self-passivating plasma-facing material for first-wall application.

Thermo-shock tests at JUDITH-1 to simulate conditions under 100 mitigated disruptions in a DEMO-like device resulted in chipping of part of the surface of the as-HIPed W-10Cr-2Ti alloy. An additional TT at 1600°C (1873 K) improves the thermo-shock resistance of this alloy since no chipping is observed but only crack formation. This improvement is due to the absence of the second (αCr,W) bcc phase which induces misfit strains and thermal stresses during repeated thermo-shock loading.

Acknowledgments

This work has been carried out within the framework of the EUROfusion Consortium and has received funding from the Euratom research and training programme 2014-2018 under grant agreement No 633053 and by the Basque Government (ELKARTEK KK-2015/00101). The views and opinions expressed herein do not necessarily reflect those of the European Commission.

References

[1] D. Maisonnier, et al., A Conceptual Study of Commercial Fusion Power Plants (2005) Final Report EFDA-RP-RE-5.0.
[2] D. Stork, et al., Fusion Eng. Des. 89 (2014) 1586–1594.
[3] N.P. Taylor, R. Pampin, Fusion Eng. Des. 81 (2006) 1333–1338.
[4] P. López-Ruiz, F. Koch, N N. Ordás, S. Linding, C. García-Rosales, Fusion Eng. Des. 86 (2011) 1719–1723.
[5] A. Calvo, N. Ordás, I. Iturriza, J.Y. Pastor, E. Tejado, T. Palacios, C. García-Rosales, Phys. Scr. (2015).
[6] P. López-Ruiz, et al., J. Nucl. Mater. 442 (2013) S219–S224.
[7] F. Koch, S. Köppl, H. Bolt, J. Nucl. Mater 386–388 (2009) 572–574.
[8] F. Koch, J. Brinkmann, S. Lindig, T.P. Mishra, Ch. Linsmeier, Phys. Scr. T145 (2011) 014019 (5 pp).
[9] C. García-Rosales, P. López-Ruiz, S. Alvarez-Martín, A. Calvo, N. Ordás, F. Koch, J. Brinkmann, Fusion Eng. Des. 89 (2014) 1611–1616.
[10] K.L. Wilson, A.E. Pontau, J. Nucl. Mater. 93-94 (1980) 569–574.
[11] T. Suresh, A. Patra, M. Sankaranarayana, R. Mitra, S.K. Pabi, Int. J. Refract. Met. H. 36 (2013) 191–203.
[12] Y. Zhou, Q.X. SuN, Z.M. Xie, R. Liu, X.P. Wang, Q.F. Fang, C.S. Liu, J. Alloy Compd. 585 (2014) 771–775.
[13] J. Brinkmann, IPP Garching, private communication.
[14] T. Wegener, A. Litnovsky, J. Binkmann, F. Koch and Ch. Linsmeier, Development of yttrium-containing self-passivating tungsten alloys for future fusion power plants, Nuclear Mater. Energy, 2016.
[15] M. Zhao, Z. Zhou, J. Tan, M. Zhong, Q. Ding, Mater. Sci. Eng. A 618 (2014) 575–577.
[16] L. Veleva, R. Schaeublin, M. Battabyal, T. Plociski, N. Baluc, Int. J. Refract. Met. H. 50 (2015) 210–216.
[17] M. Zhao, Z. Zhou, Q. Ding, M. Zhong, K. Arshad, Int. J. Refract. Met. H. 48 (2015) 19–23.
[18] W-Cr phase diagram, Bulletin of Alloy Phase Diagrams Vol. 5 No. 3 1984
[19] H. Greuner, B. Boeswirth, J. Boscary, P. McNeely, J. Nucl. Mater 367–370 (2007) 1444–1448.
[20] R. Duwe, W. Kuehnlein, H. Muenstermann, Fusion Technol. (1995) 355–358.
[21] L. Vegard, Z. Phys. 5 (1921) 17.
[22] E. Lassner, W. Schubert, Tungsten, Properties, Chemistry, Technology of the Element, Alloys and Chemical Compounds, Vienna University of Technology, Austria, 1998.
[23] J. Reiser, et al., Int. J. Refract. Met. H. 54 (2016) 351–369.
[24] B. Gludovatz, S. Wurster, T. Weingartner, A. Hoffmann, R. Pippan, Philos. Mag. 91 (2011) 3006–3020.
[25] U.K. Vashi, R.W. Armstrong, G.E. Zima, Metall. Trans. 1 (1970) 1769–1771.